Hindawi Publishing Corporation
Journal of Control Science and Engineering
Volume 2014, Article ID 989717, 13 pages
http://dx.doi.org/10.1155/2014/989717

Research Article

Adaptive Backstepping Controller Design for Leveling Control of an Underwater Platform Based on Joint Space

Zhi-Lin Zeng, Guo-Hua Xu, Yin Zhao, and Fei Xie

School of Naval Architecture and Ocean Engineering, Huazhong University of Science and Technology, Wuhan 430074, China

Correspondence should be addressed to Guo-Hua Xu; hustxu@vip.sina.com

Received 17 September 2013; Revised 4 February 2014; Accepted 5 February 2014; Published 24 March 2014

Academic Editor: Zoltan Szabo

This paper focuses on high precision leveling control of an underwater heavy load platform, which is viewed as an underwater parallel robot on the basis of its work pattern. The kinematic of platform with deformation is analyzed and the dynamics model of joint space is established. An adaptive backstepping controller according to Lyapunov's function is proposed for leveling control of platform based on joint space. Furthermore, the "lowest point fixed angle error" leveling scheme called "chase" is chosen for leveling control of platform. The digital simulation and practical experiment of single joint space actuator are carried out, and the results show high precision servo control of joint space. On the basis of this, the platform leveling control simulation relies on the hardware-in-loop system. The results indicate that the proposed controller can effectively restrain the influence from system parameter uncertainties and external disturbance to realize high precision leveling control of the underwater platform.

1. Introduction

An underwater parallel heavy-load platform based on tension-leg platform is proposed here, and it will be used to carry some special underwater tools for underwater experiments at designated depth. From the viewpoint of topology, the platform can be seen as an underwater flexible parallel robot with advantages of both parallel mechanism and flexible-driven mode. From the viewpoint of control, the platform is a multi-input and multioutput (MIMO) nonlinear system with complex coupling dynamic. Hence, it has certain difficulty to realize the high precision leveling control of platform.

At present, the studies on underwater parallel robot control are relatively lacking, so it can be just referred to rigid platform leveling control and flexible parallel robot control technology. The leveling control technology is widely used in engineering machinery, aerospace, military engineering, and other aspects, and its precision will directly affect the accuracy of overall system. Zhai and Ni proposed two leveling methods, respectively, based on position error and angle error aiming at the leveling issue of six supports hydraulic platform on stationary base [1]. Sheng and Qiu designed six-support hydraulic Stewart platform bearing heavy load, proposed computer parameterization leveling algorithm, and constructed electrohydraulic servo automatic leveling system [2, 3]. Ye focused on leveling control of the six-support platform bearing heavy load and then put forward a leveling scheme called "fixed point" scheme [4]. Zhang chose a "highest point fixed" leveling scheme called "chase" for a four-support platform and constructed the platform leveling system with programmable logic controller (PLC) [5]. Besides, many scholars have done a lot of research on the flexible parallel robot. Landsberger from Massachusetts Institute of Technology (MIT) first proposed a cable-controlled three degrees-of-freedom (DOF) parallel link manipulator and carried out dynamic analysis and control technology of system [6]. Fang et al. designed the nonlinear feed-forward control law for motion control of a six DOF tendon-based parallel manipulator [7]. Yamamoto et al. studied the dynamics and control of a parallel mechanism where an end-effector was suspended by multiple wires [8]. Pham et al. studied the workspace of a cable-driven parallel mechanism [9]. Zi gave out the mechanics analysis and control of the feed tracking system for the five-hundred meter aperture spherical radio telescope (FAST), established the dynamics models of the

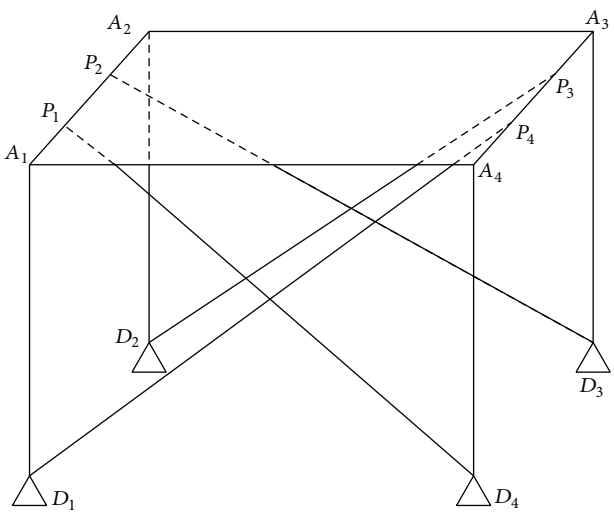

Figure 1: Platform structure.

end-effector and the drive system, respectively, and then carried out the scaled model experiment of system [10].

The existing parallel robot control applying in engineering design can be divided into two categories: one is joint space based control and another is task space based control; both have their certain advantages and disadvantages. Joint space based control mainly relies on kinematic relation of the parallel platform mechanism, as well as dynamics model of the driving devices; task space based control, however, requires dynamics' analysis of the platform to build the dynamics model of the platform [11]. Considering the complexity of the underwater platform system and unknown factors of underwater environment, accurate dynamics model of the underwater platform is hard to obtain; therefore, joint space based control is applied in order to accomplish underwater platform controller design in this paper. Given that the driving device of the platform is hydraulic winch, by using the accurate position servo control toward hydraulic winch, depth setting and orientation adjustment of the underwater platform can be realized. As to practical applications, the strong nonlinearity, as well as the uncertainty of both internal parameters and external load force of hydraulic servo system, has contributed great difficulties to the leveling control system design. Therefore many scholars have proposed various control algorithms in order to make profound study and thus to achieve the precise control of the platform.

Adaptive backstepping design based on Lyapunov's function is an effective and systematic method for nonlinear system controller design. The original backstepping control methods are designed for nonlinear systems with strict parameter feedbacks. Guan et al. provided a standard method of backstepping design to develop the controller [12–14]. In the process, however, since the controller contains the parameters adaptive law, while adaptive law also contains control variables, the system performance consequently degrades in such loop nest. Ruan et al. made the assumption that the initial coefficient value remained to be 1 or invariable before any system control input; such a system was seldom used in practical control system; instead a variety of nonlinear systems with nonstrict parameter feedbacks are usually applied in practical application; also the coefficients before system control input remained to be uncertain at most of the cases [15, 16].

In this paper, according to positioning mode of the platform, based on the kinematic and dynamic analysis of system, the joint space based control model is established. Then, an improved adaptive backstepping control method is proposed based on Lyapunov's function for the single driven joint to overcome the influence from uncertain parameters of system. Besides, we verify the performance of the proposed controller through digital simulations and individual experiments with single driven joint (an actual hydraulic winch). Finally, based on the proposed leveling scheme, the leveling control simulations of platform rely on the hardware-in-loop simulation system.

2. System Description

The underwater platform mainly consists of platform ontology, hydraulic winches, wire ropes, and gravity anchors as shown in Figure 1.

Four tension winches are installed at points A_1, A_2, A_3, and A_4 and four mooring winches are installed at points P_1, P_2, P_3, and P_4, respectively. Platform ontology always has positive buoyancy with ballast tank. All winches are connected to four gravity anchors through cables which are served as tension leg to keep the platform steady under water. Four depth transducers are installed at four corners of the platform deck, respectively, and an orientation transducer is installed at the center of the platform deck. It acquires depth and orientation information of the underwater platform with high precision transducers; then, it controls the platform based on the theory of parallel robot. The platform can realize high precision positioning at designated depth and meet the orientation requirement of carrying mechanism in certain workspace.

Both platform ontology and wire rope have a certain amount of deformation with external load. The deformation of platform cannot be ignored because of the large size, and it will be compensated during kinematics analysis. The wire rope is always tensioning with work load in the process of leveling control. As a result of this, the deformation of wire rope is constant, so its variation is ignored in this paper.

Hardware-in-loop simulation is a kind of technology which joins actual controller and model of the control object on the computer together for experiment. Complex systems like the platform require a certain building period, but its control system needs to be designed a priori. As a result of this, it can only rely on the simulation without actual control object. During the design process of the platform's control system, we utilize the hardware-in-loop simulation system (see Figure 2) to simulate the actuator (hydraulic winch) and the object (underwater platform). It will effectively shorten the building period and avoid the waste of resources to a certain extent.

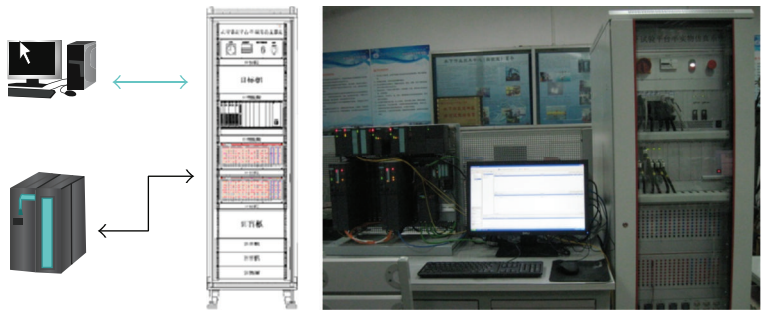

Figure 2: Hardware-in-loop simulation system.

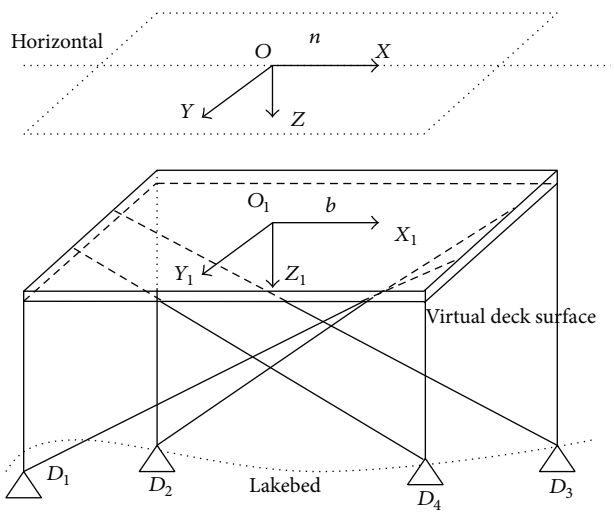

Figure 3: Underwater platform coordinate frame selection.

3. Kinematic Analysis of Underwater Platform

3.1. Coordinate Frames' Selection. Kinematic analysis of the platform requires two coordinate frames as indicated in Figure 3. The earth-fixed coordinate frame $OXYZ$ takes the horizontal plane as datum known as n-coordinate frame. Due to the deformation of platform, the actual deck is a curve surface, and it should be compensated into a flat surface which is called "virtual deck surface." The body-fixed coordinate frame $O_1X_1Y_1Z_1$ takes "virtual deck surface" as datum and its geometric center as origin known as b-coordinate frame, where the geometric centers of actual deck and virtual deck are coincident.

The platform viewed as rigid body is a six DOF parallel robot as shown in Figure 3. Owing to special positioning mode, the movement along X_1-axis and Y_1-axis and the rotation around Z_1 are limited, so the platform is a three DOF underwater parallel robot actually. In this system the position and orientation of the platform are represented by six parameters which contain coordinate values $O_1(x, y, z)$ of the origin of the b-coordinate frame and Euler angles (ϕ, θ, ψ) of the b-coordinate frame relative to the n-coordinate frame, where (ϕ, θ, ψ) represent roll angle and pitch and yaw angles. We select $(x, y, z, \phi, \theta, \psi)$ as generalized coordinates of the platform [17].

3.2. Kinematic Analysis. Let Δ_i $(i = 1, 2, \ldots, 4)$ denote the deformations of four corners on platform, and the values of depth transducers are h_i $(i = 1, 2, \ldots, 4)$, so the depth of O_1 is $h_{O1} = (1/4)((h_1 - \Delta_1) + (h_2 - \Delta_2) + (h_3 - \Delta_3) + (h_4 - \Delta_4))$. Besides, the work depth of platform is h.

Let a, b, c denote the length, width, and height of the platform, respectively; the coordinate values of A_i $(i = 1, 2, \ldots, 4)$ in the b-coordinate frame $O_1X_1Y_1Z_1$ are acquired as follows based upon the geometrical relationship:

$$\begin{aligned} {}^bA_1 &= \left(-\frac{a}{2} \quad \frac{b}{2} \quad \Delta_1\right)^T, \\ {}^bA_2 &= \left(-\frac{a}{2} \quad -\frac{b}{2} \quad \Delta_2\right)^T, \\ {}^bA_3 &= \left(\frac{a}{2} \quad -\frac{b}{2} \quad \Delta_3\right)^T, \\ {}^bA_4 &= \left(\frac{a}{2} \quad \frac{b}{2} \quad \Delta_4\right)^T. \end{aligned} \tag{1}$$

The coordinate value of arbitrary point named P in b-coordinate frame is ${}^bP$, and ${}^nP$ denotes the coordinate value of point P in n-coordinate frame. ${}^n_bR$ is the rotation matrix of b-coordinate with respect to n-coordinate. ${}^nP_b$ $(0, 0, h_{O1})$ is the coordinate value of b-coordinate origin in n-coordinate. Then (2) is acquired as follows:

$${}^nP = {}^n_bR \cdot {}^bP + {}^nP_b, \tag{2}$$

where

$${}^n_bR = \begin{bmatrix} \cos\theta\cos\psi & \sin\phi\sin\theta\cos\psi - \cos\phi\sin\psi & \cos\phi\sin\theta\cos\psi + \sin\phi\sin\psi \\ \cos\theta\sin\psi & \sin\phi\sin\theta\sin\psi + \cos\phi\cos\psi & \cos\phi\sin\theta\sin\psi - \sin\phi\cos\psi \\ -\sin\theta & \sin\phi\cos\theta & \cos\phi\cos\theta \end{bmatrix}. \tag{3}$$

The coordinate values of A_i in n-coordinate frame can be acquired based upon coordinate transformation as follows:

$$
\begin{aligned}
{}^{n}A_1 &= \begin{bmatrix} -\frac{a}{2}\cos\theta\cos\psi + \frac{b}{2}\sin\phi\sin\theta\cos\psi - \frac{b}{2}\cos\phi\sin\psi + \Delta_1\cos\phi\sin\theta\cos\psi + \Delta_1\sin\phi\sin\psi \\ -\frac{a}{2}\cos\theta\sin\psi + \frac{b}{2}\sin\phi\sin\theta\sin\psi + \frac{b}{2}\cos\phi\cos\psi + \Delta_1\cos\phi\sin\theta\sin\psi - \Delta_1\sin\phi\cos\psi \\ h_{O1} + \frac{a}{2}\sin\theta + \frac{b}{2}\sin\phi\cos\theta + \Delta_1\cos\phi\cos\theta \end{bmatrix}, \\
{}^{n}A_2 &= \begin{bmatrix} -\frac{a}{2}\cos\theta\cos\psi - \frac{b}{2}\sin\phi\sin\theta\cos\psi + \frac{b}{2}\cos\phi\sin\psi + \Delta_2\cos\phi\sin\theta\cos\psi + \Delta_2\sin\phi\sin\psi \\ -\frac{a}{2}\cos\theta\sin\psi - \frac{b}{2}\sin\phi\sin\theta\sin\psi - \frac{b}{2}\cos\phi\cos\psi + \Delta_2\cos\phi\sin\theta\sin\psi - \Delta_2\sin\phi\cos\psi \\ h_{O1} + \frac{a}{2}\sin\theta - \frac{b}{2}\sin\phi\cos\theta + \Delta_2\cos\phi\cos\theta \end{bmatrix}, \\
{}^{n}A_3 &= \begin{bmatrix} \frac{a}{2}\cos\theta\cos\psi - \frac{b}{2}\sin\phi\sin\theta\cos\psi + \frac{b}{2}\cos\phi\sin\psi + \Delta_3\cos\phi\sin\theta\cos\psi + \Delta_3\sin\phi\sin\psi \\ \frac{a}{2}\cos\theta\sin\psi - \frac{b}{2}\sin\phi\sin\theta\sin\psi - \frac{b}{2}\cos\phi\cos\psi + \Delta_3\cos\phi\sin\theta\sin\psi - \Delta_3\sin\phi\cos\psi \\ h_{O1} - \frac{a}{2}\sin\theta - \frac{b}{2}\sin\phi\cos\theta + \Delta_3\cos\phi\cos\theta \end{bmatrix}, \\
{}^{n}A_4 &= \begin{bmatrix} \frac{a}{2}\cos\theta\cos\psi + \frac{b}{2}\sin\phi\sin\theta\cos\psi - \frac{b}{2}\cos\phi\sin\psi + \Delta_4\cos\phi\sin\theta\cos\psi + \Delta_4\sin\phi\sin\psi \\ \frac{a}{2}\cos\theta\sin\psi + \frac{b}{2}\sin\phi\sin\theta\sin\psi + \frac{b}{2}\cos\phi\cos\psi + \Delta_4\cos\phi\sin\theta\sin\psi - \Delta_4\sin\phi\cos\psi \\ h_{O1} - \frac{a}{2}\sin\theta + \frac{b}{2}\sin\phi\cos\theta + \Delta_4\cos\phi\cos\theta \end{bmatrix}.
\end{aligned}
\tag{4}
$$

During the whole diving process, the orientation of platform is monitored to ensure steadiness. Hence, the roll and pitch angles of the platform are small ($|\phi, \theta| \leq 5^\circ$), so the angle δ is small, as shown in Figure 4. Then, it realizes the leveling control of the platform based on orientation information of the platform measured by high precision orientation transducer. A_i represents the position before adjustment, B_i represents the ideal position after adjustment, and D_i represents the position of anchor.

The Jacobian matrix of flexible parallel robot is defined as the linear relation between the velocity of the driven cable and the velocity of the platform [18]. In order to calculate the Jacobian matrix, it is assumed that the bottom of the test water area is generally flat, and the depth is H. The coordinate values of D_i in n-coordinate frame are shown as follows:

$$
\begin{aligned}
{}^{n}D_1 &= \left(-\frac{a}{2} \quad \frac{b}{2} \quad H\right)^T, \\
{}^{n}D_2 &= \left(-\frac{a}{2} \quad -\frac{b}{2} \quad H\right)^T, \\
{}^{n}D_3 &= \left(\frac{a}{2} \quad -\frac{b}{2} \quad H\right)^T, \\
{}^{n}D_4 &= \left(\frac{a}{2} \quad \frac{b}{2} \quad H\right)^T.
\end{aligned}
\tag{5}
$$

The length vector $l_i = A_iD_i$ expressed with respect to n-coordinate frame can be computed by

$$
\vec{l}_i = \vec{r}_{A_i} - \vec{r}_{D_i} \quad (i = 1, 2, 3, 4). \tag{6}
$$

We define $\dot{l} = \left[\dot{l}_1 \ \dot{l}_2 \ \dot{l}_3 \ \dot{l}_4\right]^T$ as the velocity of the driven cable and specify the velocity of the platform as $\dot{r}_{O_1}$ represented by translation along three axes and rotation around three axes of the b-coordinate frame as shown in

$$
\begin{aligned}
\dot{l} &= J \cdot \dot{r}_{O_1}, \\
\dot{r}_{O_1} &= \left[\dot{x} \ \dot{y} \ \dot{z} \ \dot{\phi} \ \dot{\theta} \ \dot{\psi}\right]^T,
\end{aligned}
\tag{7}
$$

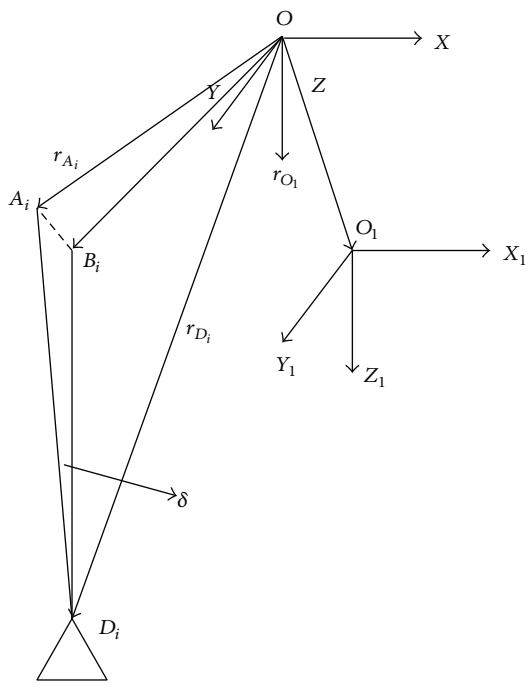

Figure 4: Orientation adjustment diagram.

where Jacobian matrix J is

$$J = \begin{bmatrix} \frac{\partial l_i}{\partial x} & \frac{\partial l_i}{\partial y} & \frac{\partial l_i}{\partial z} & \frac{\partial l_i}{\partial \phi} & \frac{\partial l_i}{\partial \theta} & \frac{\partial l_i}{\partial \psi} \end{bmatrix} \quad (i = 1, 2, \ldots, 4). \tag{8}$$

Proved by the calculation, the Jacobian matrix is always nonsingular in the workspace of the platform ($|\phi, \theta| \leq 5°$).

Actually, the lakebed environment is unknown, so the calculation result of cable length above is just an estimated value which is not precise enough for leveling control of platform. As the platform moves nearby the horizontal position, we take an approximate method for the calculation of cable length as follows:

$$\|D_i A_i\| = \|D_i B_i\| + \|A_i B_i\|. \tag{9}$$

The variation of cable i length $\Delta l_i = B_i A_i$ expressed with respect to n-coordinate frame can be computed by

$$\Delta \left\| \vec{l}_i \right\| = \left\| \vec{r}_{B_i} - \vec{r}_{A_i} \right\| \quad (i = 1, 2, 3, 4). \tag{10}$$

The coordinate values of B_i in n-coordinate frame are denoted as follows:

$$\begin{aligned} {}^nB_1 &= \left(-\frac{a}{2} \quad \frac{b}{2} \quad h - \Delta_1\right)^T, \\ {}^nB_2 &= \left(-\frac{a}{2} \quad -\frac{b}{2} \quad h - \Delta_2\right)^T, \\ {}^nB_3 &= \left(\frac{a}{2} \quad -\frac{b}{2} \quad h - \Delta_3\right)^T, \\ {}^nB_4 &= \left(\frac{a}{2} \quad \frac{b}{2} \quad h - \Delta_4\right)^T. \end{aligned} \tag{11}$$

4. Dynamic Modeling of Joint Space

4.1. Dynamic Modeling of Underwater Platform. The dynamical equations can be obtained based on the Newton-Euler method as shown in

$$\begin{aligned} m\ddot{x} &= M + F_a, \\ I\dot{\Omega} + \Omega \times (I\Omega) &= M_g + M_a, \end{aligned} \tag{12}$$

where $x = [x \ y \ z]^T$ is the position vector of the b-coordinate frame origin with respect to the n-coordinate frame, m is the mass of the platform with ballast tank full of water, Ω is angular velocity of the b-coordinate frame, M is the gravity and buoyancy of the platform with ballast tank full of water, and I is the moment of inertia of the platform in the n-coordinate frame; then $I = {}^n_bR I_{O1} {}^n_bR^T$, M_g is the gravity and buoyancy torque of the platform, and F_a and M_a are the external force and torque, respectively. The moment of inertia of the platform in b-coordinate frame is expressed in [19, 20]

$$I_{O1} = \begin{bmatrix} I_{xx} & -I_{xy} & -I_{xz} \\ -I_{yx} & I_{yy} & -I_{yz} \\ -I_{zx} & -I_{zy} & I_{zz} \end{bmatrix}. \tag{13}$$

Here, it is supposed that the mass of the platform is uniformly distributed, so the center of gravity $G(x_g, y_g, z_g)$ is geometric center of platform, and the center of buoyancy $B(x_b, y_b, z_b)$ is located right above the center of gravity.

Through a series of transformations and substitutions, the dynamics model of the platform is expressed in terms of η generalized coordinates as the following general form [21]:

$$\begin{aligned} M(\eta)\ddot{\eta} + C(\eta, \dot{\eta})\dot{\eta} + D(\eta, \dot{\eta})\dot{\eta} + G(\eta) + d_\eta &= F, \\ \dot{\eta} = J(\eta)\nu, \qquad F &= -J^T\tau, \end{aligned} \tag{14}$$

where η denotes the position and orientation vectors with coordinates in the n-coordinate frame, ν denotes the linear and angular velocity vectors with coordinates in the b-coordinate frame, $M(\eta)$ is the inertia matrix of the platform (including added mass), $C(\eta, \dot{\eta})$ is the matrix of Coriolis and centripetal terms (including added mass), $D(\eta, \dot{\eta})$ is the damping matrix of the platform, $G(\eta)$ is vector of gravitational forces and torques, and d_η is the vector of external disturbance terms. Here, F is the force and torque vector generated by winch, and τ is the vector of control inputs by tensile force of cables. The transformation matrix is shown as follows:

$$J(\eta) = \begin{bmatrix} R_b^n(\Theta) & 0_{3\times3} \\ 0_{3\times3} & T_\Theta(\Theta) \end{bmatrix}, \tag{15}$$

where

$$R_b^n(\Theta) = {}_b^nR, \qquad R_b^n(\Theta)^{-1} = R_b^n(\Theta)^T,$$

$$T_\Theta(\Theta) = \begin{bmatrix} 1 & \sin\phi\tan\theta & \cos\phi\tan\theta \\ 0 & \cos\phi & -\sin\phi \\ 0 & \dfrac{\sin\phi}{\cos\theta} & \dfrac{\cos\phi}{\cos\theta} \end{bmatrix}, \tag{16}$$

$$T_\Theta^{-1}(\Theta) = \begin{bmatrix} 1 & 0 & -\sin\theta \\ 0 & \cos\phi & \cos\theta\sin\phi \\ 0 & -\sin\phi & \cos\theta\cos\phi \end{bmatrix}.$$

It is difficult to establish an accurate dynamics model for the platform due to the nonlinear characteristic of the overall system, complicated underwater environment, and many other uncertainties. Considering the low velocity of the platform underwater, we utilize the method based on joint space to realize the control of the platform.

4.2. Dynamic Modeling of Driving System. Considering the underwater dynamic sealing and heavy load, the hydraulic driving mode is chosen for the system. The hydraulic system adopts valve control with quantitative pump and motor for power supply, as well as keeping running smooth in overrunning load condition with respect to the balance valve. The driving system of platform is mainly composed of oil source, electrohydraulic servo valve, hydraulic motor, servo amplifier, and load as shown in Figure 5.

The dynamics model of hydraulic system is mainly composed of the following three equations [22]. In this section, we introduce a nonlinear mathematic model of the system.

The flow equation of servo valve is described as

$$Q_L = C_d\omega x_v\sqrt{\frac{1}{\rho}\left(P_S - P_L\operatorname{sgn}(x_v)\right)}, \tag{17}$$

where Q_L is the load flow, C_d is the discharge coefficient, ω is the area gradient, x_v is the displacement of the spool in the servo valve, P_S is the supply pressure of the pump, P_L is the load pressure, and ρ is the hydraulic oil density.

The continuity equation of the motor is

$$Q_L = D_m\dot{\theta}_m + C_{tm}P_L + \frac{V_m}{4\beta_e}\dot{P}_L, \tag{18}$$

where D_m is the volumetric displacement of the hydraulic motor, θ_m is the rotor angle of motor rotor, C_{tm} is the total leakage coefficient, V_m is the total actuator volume, and β_e is the effective bulk modulus of the system.

As the servo valve dynamics are often sufficiently fast, they can be ignored in this paper. Therefore

$$K_1 = \frac{i}{u}, \qquad K_2 = \frac{x_v}{i}, \tag{19}$$

where K_1 is the servo amplifier gain, K_2 is the servo valve gain, u is the controller output voltage, and i is the input current of the servo valve.

The platform can be viewed as a rigid body, so the load torsional spring stiffness $G = 0$. The torque balance equation of the motor is

$$T_s = D_mP_L = J_m\ddot{\theta}_m + B_m\dot{\theta}_m + T_L, \tag{20}$$

where T_s is the torque generated by hydraulic motor, J_m is the inertia of hydraulic motor and load, B_m is the viscous damping coefficient of hydraulic motor and load, and T_L is the external load torque.

4.3. Dynamic Modeling of Joint Space. The driving system of the platform is hydraulic winch which consists of hydraulic motor, reducer, and capstan. Cables with high modulus of elasticity are selected, so elastic deformation is negligible. The relation between length variation of cable and rotor angle of motor is shown as follows:

$$\theta_m = \frac{n\cdot\Delta\|l\|}{r}, \tag{21}$$

where θ_m denotes the rotor angle of motor, r denotes radius of the capstan, n denotes reduction ratio, and $\Delta\|l\|$ denotes the length variation of cable.

Then $\dot{\theta}_m = (n/r)\cdot\dot{l}$, $\ddot{\theta}_m = (n/r)\cdot\ddot{l}$.

With Jacobian matrix, we can acquire

$$\dot{\eta} = \left(\frac{r}{n}\right)J^{-1}\dot{\theta}_m, \qquad \ddot{\eta} = \left(\frac{r}{n}\right)\left(\dot{J}^{-1}\dot{\theta}_m + J^{-1}\ddot{\theta}_m\right). \tag{22}$$

So, dynamics equation of the platform can be transformed from task space to joint space as shown in

$$A'\ddot{\theta}_m + B'\dot{\theta}_m + G' + T_d' = T'. \tag{23}$$

Here, A' is equivalent inertia matrix of joint space, and B' is equivalent viscous damping coefficient matrix of joint space. The coefficients of (23) are expressed as

$$\begin{aligned} A' &= \left(\frac{r^2}{n}\right)J^{-T}M(\eta)J^{-1}, \\ T_d' &= r\cdot J^{-T}d_\eta, \qquad T' = -r\cdot\tau, \\ B' &= \left(\frac{r^2}{n}\right)\cdot\left(J^{-T}M(\eta)\dot{J}^{-1} + J^{-T}C(\eta,\dot{\eta})J^{-1}\right. \\ &\qquad \left. + J^{-T}D(\eta,\dot{\eta})J^{-1}\right)G' \\ &= r\cdot J^{-T}G(\eta). \end{aligned} \tag{24}$$

The platform moves nearby the horizontal position. As a result of this, we define the value of A' as $A_0 = [a_{0ij}]_{4\times4}$ when the platform is in the horizontal position. The dynamical equation matrix of the platform joint space is shown in

$$\begin{aligned} &\left[a_{ij}\right]_{4\times4}\cdot\ddot{\theta}_{m4\times1} + \left[b_{ij}\right]_{4\times4}\cdot\dot{\theta}_{m4\times1} \\ &\quad + \left[g_i\right]_{4\times1} + \left[t_{d_i}\right]_{4\times1} = \left[t_i\right]_{4\times1} \quad (i,j = 1,2,3,4). \end{aligned} \tag{25}$$

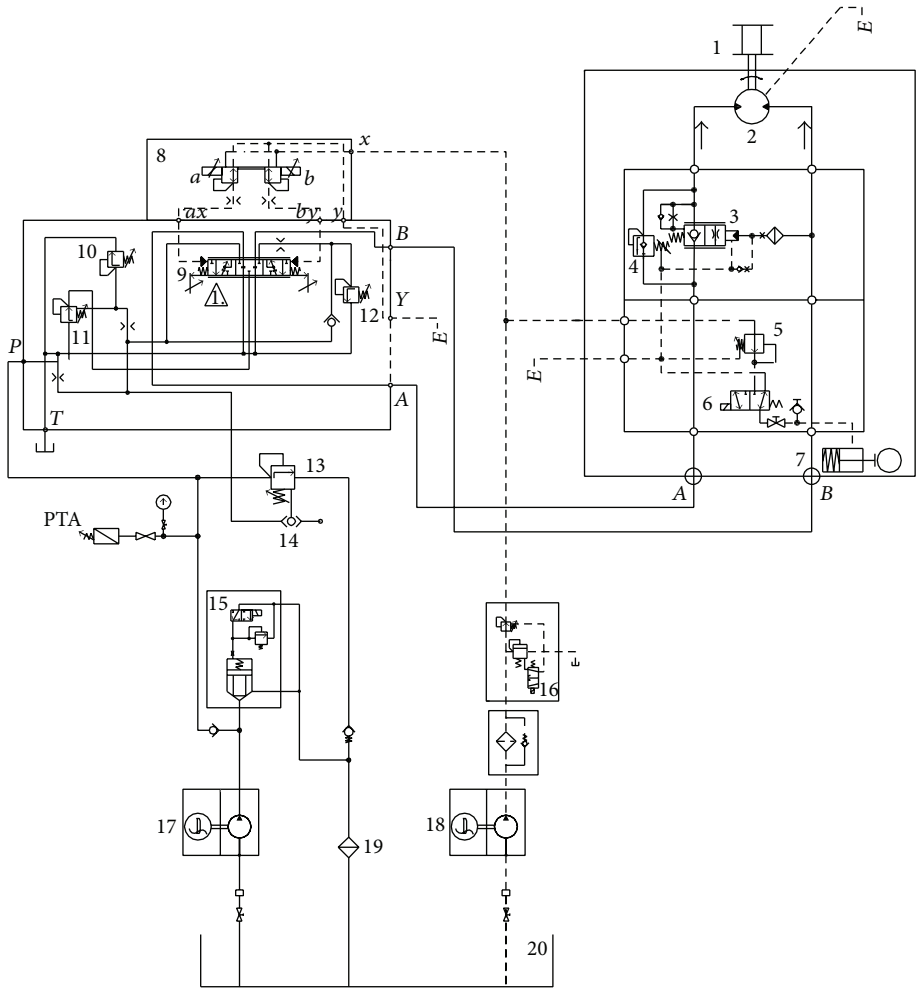

Figure 5: Hydraulic principle diagram of the winch.

As to build driving branches controlling dynamics model of inverse dynamics of the platform, we rewrite (23) as shown in

$$a_{0ii} \cdot \ddot{\theta}_{m_i} + b_i \cdot \dot{\theta}_{m_i} + F_i{}' = t_i \quad (i = 1, 2, 3, 4), \tag{26}$$

where

$$\begin{aligned} F_i{}' = {} & a_{ii} \cdot \ddot{\theta}_{m_i} + \sum_{\substack{j=1 \\ j \neq i}}^{4} a_{ij} \cdot \ddot{\theta}_{m_j} + b_{ii} \cdot \dot{\theta}_{m_i} \\ & + \sum_{\substack{j=1 \\ j \neq i}}^{4} b_{ij} \cdot \dot{\theta}_{m_j} + g_i + t_{d_i} - a_{0ii} \cdot \ddot{\theta}_{m_i} - b_i \cdot \dot{\theta}_{m_i} \end{aligned} \tag{27}$$

is viewed as dynamic coupling interference force which acts on the driving branch i.

Therefore, the dynamics model of the platform is divided into two parts: the first part is standard driving branch controlling dynamical model expressed as $a_{0ii} \cdot \ddot{\theta}_{m_i} + b_i \cdot \dot{\theta}_{m_i}$, the other part is dynamic coupling interference model that acts on the driving branch i.

Aiming at the driving branch of the platform, the torque balance equation of the motor is shown in

$$T_{s_i} = J_{m_i} \ddot{\theta}_{m_i} + B_{m_i} \dot{\theta}_{m_i} + T_{L_i} \quad (i = 1, 2, 3, 4). \tag{28}$$

On the basis of (26), inertia of hydraulic motor and load is denoted as $J_{m_i} = a_{0ii}$, viscous damping coefficient is denoted as $B_{m_i} = b_i$, external load torque which acts on the motor drive shaft is denoted as $T_{L_i} = F_i{}'$, and torque generated by hydraulic motor is denoted as $T_{s_i} = t_i$.

The trajectory of the platform is nearby the horizontal position with limited amplitude and it is far away from the singular area. Therefore, the external load torque on the motor shaft is continuous and bounded. As a result of this, the dynamic coupling torque that acts on the driving branch can be seen as external disturbance torque including inertia, damping, and gravity/buoyancy torques [23].

We aim at single tension leg during the formula derivation of joint space controller design; so the subscript i will be omitted below for convenience.

Take $x = [x_1 \quad x_2 \quad x_3] = [\theta_m \quad \dot{\theta}_m \quad T_s]$ as the state variables, where x_1 is the rotor angle of motor rotor, x_2 is the velocity of motor rotor, and x_3 is the torque generated by

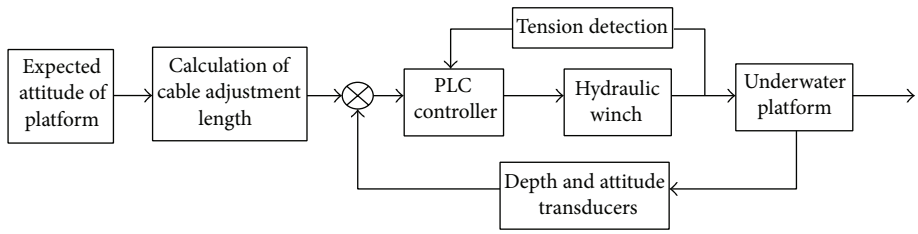

Figure 6: Control principle diagram.

hydraulic motor. The coefficient of u is written in the form of reciprocal to make the controller design convenient. The state space description for the dynamics model of joint space obtained from formulas (17)–(28) is described as

$$\begin{aligned} \dot{x}_1 &= x_2, \\ \dot{x}_2 &= a_1 x_2 + \left(\frac{1}{a_2}\right) x_3 + d, \\ \dot{x}_3 &= b_1 x_2 + b_2 x_3 + \left(\frac{1}{b_3}\right) g(x_v) u, \end{aligned} \tag{29}$$

where

$$\begin{gathered} a_1 = -\frac{B_m}{J_m}, \qquad a_2 = J_m, \\ d = -\frac{T_L}{J_m}, \qquad b_1 = -\frac{4D_m^2 \beta_e}{V_m}, \\ b_2 = -\frac{4C_{tm}\beta_e}{V_m}, \qquad b_3 = \frac{V_m \sqrt{\rho}}{4D_m \beta_e C_d \omega K_1 K_2}, \\ g(x_v) = \sqrt{P_S - P_L \operatorname{sgn}(x_v)}; \end{gathered} \tag{30}$$

u is the system input.

5. Design of Adaptive Backstepping Controller

In this paper, we mainly view the leveling control of the platform. Based on the working characteristics of the platform, the joint space based control method is chosen, so the precision of system will depend on precision of single driven joint. Besides, an improved adaptive backstepping control method is proposed based on Lyapunov's function for the single driven joint to overcome the influence from uncertain parameters of system. In order to avoid the overrunning load condition of hydraulic system, the "lowest point fixed angle error" leveling scheme called "chase" is chosen for the leveling control of platform. This leveling scheme means that we keep the lowest point fixed and adjust the other points to make the roll angle of platform tend to zero first and then adjust the pitch angle to zero in the same way, so as to realize the leveling of platform ultimately. The control principle diagram is shown in Figure 6.

With the joint space control method, we design adaptive backstepping controller for single driven joint of the system and give adaptive law of the uncertain coefficients based on Lyapunov's stability theory [24–28]. In the following derived process, x_i $(i = 1, 2, 3)$ are the real values of system state variables, x_{id} $(i = 1, 2, 3)$ are the expectation values of system state variables, and $c_i > 0$ $(1, 2, 3)$ are the controller parameters.

Joint space controller design: firstly, define error as follows:

$$e_1 = x_1 - x_{1d}. \tag{31}$$

Differentiate (31) as follows:

$$\dot{e}_1 = \dot{x}_1 - \dot{x}_{1d} = x_2 - \dot{x}_{1d}. \tag{32}$$

So there is a Lyapunov function as follows:

$$V_1 = \frac{1}{2} e_1^2 \geq 0. \tag{33}$$

Differentiating (33) gives us

$$\dot{V}_1 = e_1 \dot{e}_1 = e_1 (x_2 - \dot{x}_{1d}). \tag{34}$$

Define error e_2 as

$$e_2 = x_2 - x_{2d}, \tag{35}$$

where x_{2d} is the first virtual control variable. Consider

$$x_{2d} = \dot{x}_{1d} - c_1 e_1. \tag{36}$$

Substituting (35) and (36) in (34) results in

$$\dot{V}_1 = -c_1 e_1^2 + e_1 e_2. \tag{37}$$

If $e_2 = 0$, then $\dot{V}_1 \leq 0$. We need to do the next step of design.

Differentiating (35) gives us

$$\dot{e}_2 = \dot{x}_2 - \dot{x}_{2d} = a_1 x_2 + \left(\frac{1}{a_2}\right) x_3 + d - \dot{x}_{2d}. \tag{38}$$

In order to avoid the nesting problem that the adaptive laws of $\hat{a}_2$ and $\hat{b}_3$ include the virtual control variable x_{3d} and u, we add coefficient in front of e_2 and e_3 during the selecting of the Lyapunov functions V_2 and V_3.

Select another Lyapunov function as follows:

$$V_2 = V_1 + \frac{1}{2} a_2 e_2^2 \geq 0. \tag{39}$$

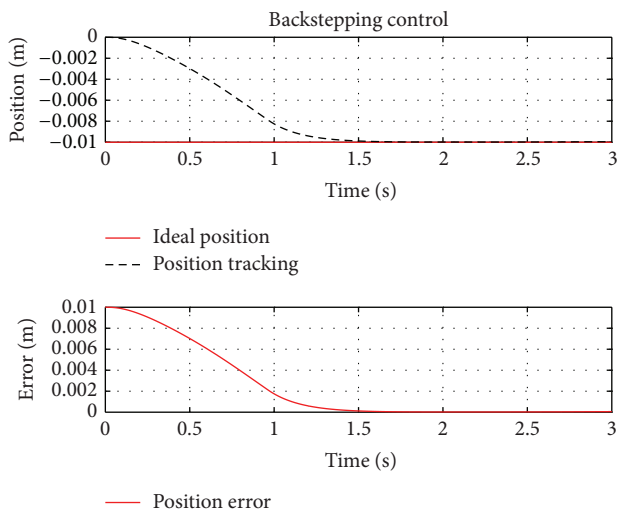

FIGURE 7: The response of adaptive backstepping controller.

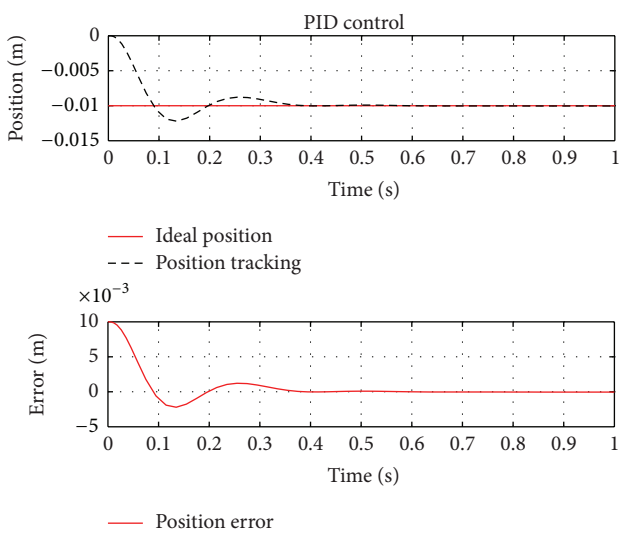

FIGURE 8: The response of PID controller.

Differentiate (39) as follows:

$$\begin{aligned}\dot{V}_2 &= e_1 e_2 - c_1 e_1^2 + a_2 e_2 \dot{e}_2 \\ &= e_1 e_2 - c_1 e_1^2 + e_2 \left(\tau_1 x_2 + x_3 + \tau_2 - a_2 \dot{x}_{2d}\right),\end{aligned} \tag{40}$$

where $\tau_1 = a_1 a_2$ and $\tau_2 = a_2 d$.

Define $\tilde{\tau}_1 = \tau_1 - \hat{\tau}_1$, $\tilde{\tau}_2 = \tau_2 - \hat{\tau}_2$, $\tilde{a}_2 = a_2 - \hat{a}_2$, and $\tilde{b}_3 = b_3 - \hat{b}_3$. Here $\hat{\tau}_1, \hat{\tau}_2, \hat{a}_2$, and $\hat{b}_3$ are the estimated values of τ_1, τ_2, a_2, and b_3.

Define the error as

$$e_3 = x_3 - x_{3d}. \tag{41}$$

Here x_{3d} is the second virtual control variable. Consider

$$x_{3d} = -e_1 - \hat{\tau}_1 x_2 - \hat{\tau}_2 + \hat{a}_2 \dot{x}_{2d} - c_2 e_2. \tag{42}$$

Substituting (41) and (42) in (40) results in

$$\dot{V}_2 = -c_1 e_1^2 - c_2 e_2^2 + e_2 e_3 + e_2 \left(\tilde{\tau}_1 x_2 + \tilde{\tau}_2 - \tilde{a}_2 \dot{x}_{2d}\right). \tag{43}$$

If $e_3 = 0$, then $\dot{V}_2 \le 0$. We need to do the next step of design.

Differentiating (41) gives us

$$\dot{e}_3 = \dot{x}_3 - \dot{x}_{3d} = b_1 x_2 + b_2 x_3 + \left(\frac{1}{b_3}\right) g\left(x_v\right) u - \dot{x}_{3d}. \tag{44}$$

Select another Lyapunov function as follows:

$$V_3 = V_2 + \frac{1}{2} b_3 e_3^2 + \frac{1}{2}\lambda_1 \tilde{\tau}_1^2 + \frac{1}{2}\lambda_2 \tilde{\tau}_2^2 + \frac{1}{2}\lambda_3 \tilde{a}_2^2 + \frac{1}{2}\lambda_4 \tilde{b}_3^2, \tag{45}$$

where $\lambda_i > 0$, $(i = 1, \ldots, 4)$.

Differentiate (45) as follows:

$$\begin{aligned}\dot{V}_3 = &- c_1 e_1^2 - c_2 e_2^2 + e_2 \left(\tilde{\tau}_1 x_2 + \tilde{\tau}_2 - \tilde{a}_2 \dot{x}_{2d}\right) \\ &+ e_3 \left(e_2 + \tau_3 x_2 + \tau_4 x_3 + g\left(x_v\right) u - b_3 \dot{x}_{3d}\right) \\ &- \lambda_1 \tilde{\tau}_1 \dot{\hat{\tau}}_1 - \lambda_2 \tilde{\tau}_2 \dot{\hat{\tau}}_2 - \lambda_3 \tilde{a}_2 \dot{\hat{a}}_2 - \lambda_4 \tilde{b}_3 \dot{\hat{b}}_3.\end{aligned} \tag{46}$$

Here $\tau_3 = b_1 b_3$ and $\tau_4 = b_2 b_3$. In this paper, we mainly consider the uncertainties of total inertia of hydraulic J_m, viscous damping coefficient B_m, and external load torque T_L, so τ_3 and τ_4 are constant.

Therefore, the output of the controller is expressed in

$$u = \frac{1}{g\left(x_v\right)} \left(-e_2 - \tau_3 x_2 - \tau_4 x_3 + \hat{b}_3 \dot{x}_{3d} - c_3 e_3\right), \tag{47}$$

where

$$\begin{aligned}\dot{x}_{3d} = &- \left(1 + \dot{\hat{\tau}}_1 + c_1 \dot{\hat{a}}_2 + a_1 c_2 + c_1 c_2 + a_1 \hat{\tau}_1 + c_1 a_1 \hat{a}_2\right) x_2 \\ &- \left(c_2 + \hat{\tau}_1 + c_1 \hat{a}_2\right) \left(\frac{1}{a_2}\right) x_3 + \left(1 + c_1 c_2 + c_1 \dot{\hat{a}}_2\right) \dot{x}_{1d} \\ &+ \left(c_1 \hat{a}_2 + c_2 + \dot{\hat{a}}_2\right) \ddot{x}_{1d} \\ &+ \hat{a}_2 \dddot{x}_{1d} - \left(c_1 \hat{a}_2 + c_2 + \hat{\tau}_1\right) d - \dot{\hat{\tau}}_2.\end{aligned} \tag{48}$$

Substituting (47) and (48) in (46) results in

$$\begin{aligned}\dot{V}_3 = &- c_1 e_1^2 - c_2 e_2^2 - c_3 e_3^2 + \tilde{\tau}_1 \left(e_2 x_2 - \lambda_1 \dot{\hat{\tau}}_1\right) \\ &+ \tilde{\tau}_2 \left(e_2 - \lambda_2 \dot{\hat{\tau}}_2\right) - \tilde{a}_2 \left(e_2 \dot{x}_{2d} + \lambda_3 \dot{\hat{a}}_2\right) \\ &- \tilde{b}_3 \left(e_3 \dot{x}_{3d} + \lambda_4 \dot{\hat{b}}_3\right).\end{aligned} \tag{49}$$

So the adaptation law is chosen as

$$\begin{aligned}\dot{\hat{\tau}}_1 &= \frac{1}{\lambda_1} e_2 x_2, \qquad \dot{\hat{\tau}}_2 = \frac{1}{\lambda_2} e_2 \\ \dot{\hat{a}}_2 &= -\frac{1}{\lambda_3} e_2 \dot{x}_{2d}, \qquad \dot{\hat{b}}_3 = -\frac{1}{\lambda_4} e_3 \dot{x}_{3d}.\end{aligned} \tag{50}$$

6. Simulation and Experiment

Firstly, digital simulation of the hydraulic system is done to prove rationality of the model and controller; secondly, an

Figure 9: The individual experiment equipments.

Figure 10: The result of wire rope draw-in at 0.01 m.

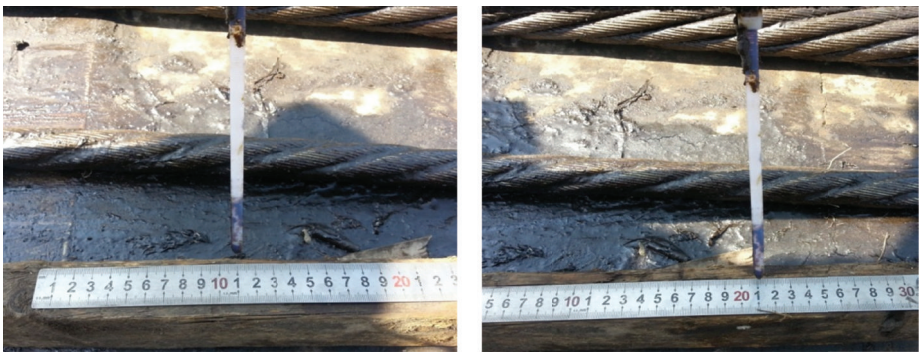

Figure 11: The result of wire rope draw-in at 0.1 m.

Figure 12: Actual controller and hardware-in-loop system.

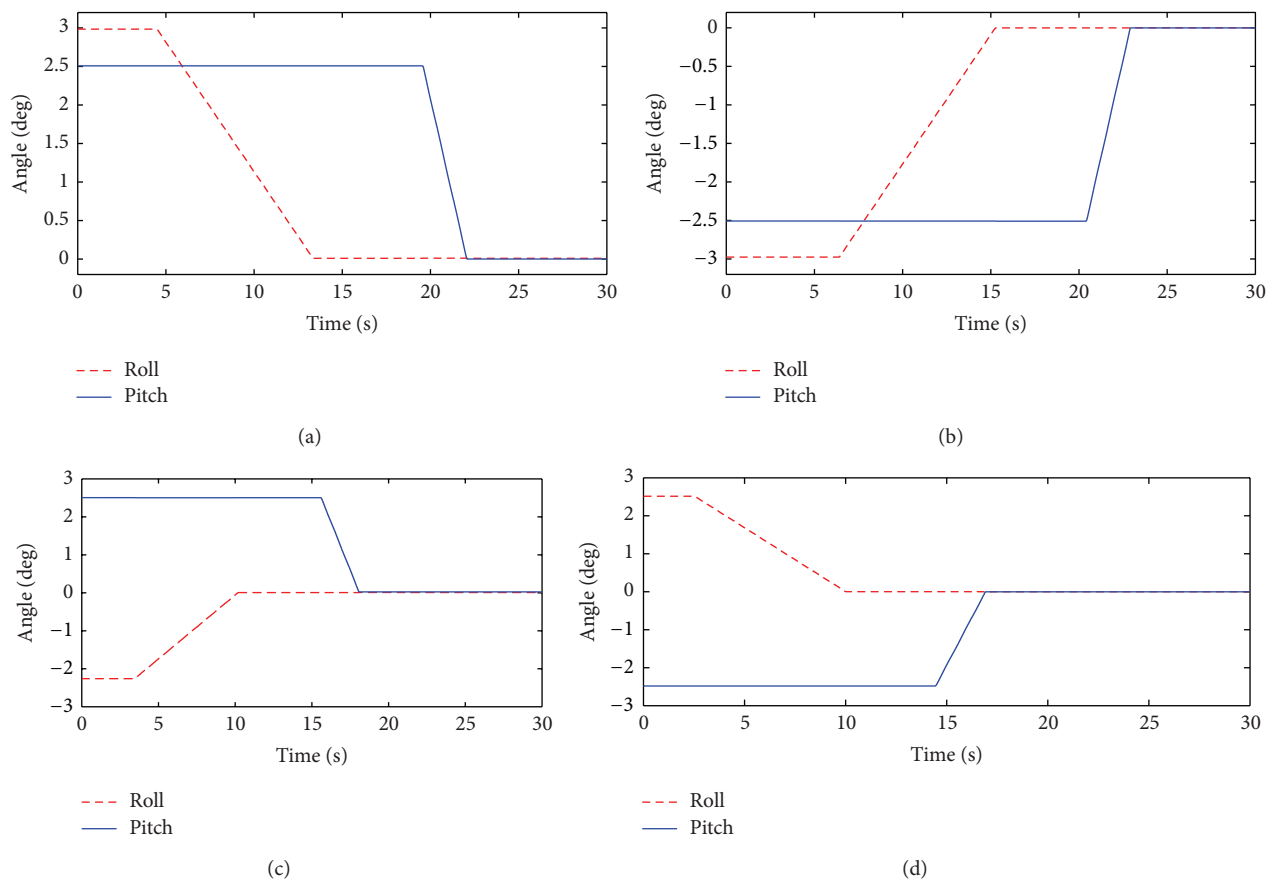

FIGURE 13: The leveling control with adaptive backstepping controller.

actual hydraulic winch is taken to perform the individual experiment based on digital simulation; then, we carry out hardware-in-loop simulation for leveling control of the platform which verifies effectiveness of the proposed control method further. According to the design of underwater platform and hydraulic winch, the primary parameters of system are given as shown in Table 1. Moment of inertia of the platform in b-coordinate frame (in $\mathrm{kg} \cdot \mathrm{m}^2$ unit):

$$I_{O1} = \begin{bmatrix} 7.29 \times 10^6 & 0 & 0 \\ 0 & 6.57 \times 10^7 & 0 \\ 0 & 0 & 6.48 \times 10^7 \end{bmatrix}. \quad (51)$$

During the practical experiment of underwater platform, the parameters of the hydraulic system will change with the changing of environment slowly, especially the external load torque on the motor. Because of the special work environment of underwater platform, the variations of platform orientation, hydrodynamic force, and flow will affect the force on the platform. Hence, we consider the hydrodynamic force and interference torque as a component of external load torque on the motor. So we mainly consider the uncertainties of total inertia of hydraulic J_m, viscous damping coefficient B_m, and external load torque T_L. It is assumed that they vary slowly with time as follows:

$$\begin{aligned} J_m &= J_{m0} + 0.1 J_{m0} \sin(2\pi t), \\ B_m &= B_{m0} + 0.1 B_{m0} \sin(2\pi t), \\ T_L &= T_{L0} + 0.2 T_{L0} \sin(2\pi t). \end{aligned} \quad (52)$$

6.1. Digital Simulation. In this section, we utilize MATLAB to compare effectiveness of the adaptive backstepping controller with conventional PID controller.

The parameters of the adaptive backstepping controller based on joint space control are as follows:

$$\begin{aligned} &c_1 = 90, \quad c_2 = 15, \quad c_3 = 90, \\ &\lambda_1 = 1 \times 10^5, \quad \lambda_2 = 4 \times 10^7, \\ &\lambda_3 = 1 \times 10^5, \quad \lambda_4 = 1 \times 10^5. \end{aligned} \quad (53)$$

The parameters of conventional PID controller are as follows:

$$K_p = 0.5, \quad K_i = 0.1, \quad K_d = 0.1. \quad (54)$$

The simulation is done with $-0.01\,\mathrm{m}$ position input which signifies the wire rope draw-in, and the results are shown in Figures 7 and 8.

Table 1: Parameters of the platform and hydraulic winch.

Parameter	Notation	Unit	Value
Length of platform	a	m	25
Width of platform	b	m	10
Height of platform	c	m	1
Work depth of platform	h	m	60
Radius of winch capstan	r	m	0.768
Reduction ratio of winch	n		536
Servo amplifier gain	K_1	A/V	0.125
Servo valve gain	K_2	m/A	0.01
Servo valve discharge coefficient	C_d		0.61
Servo valve area gradient	ω	m	0.785
Supply pressure of pump	P_S	Pa	1.5×10^7
Hydraulic oil density	ρ	kg/m^3	850
Volumetric displacement of hydraulic motor	D_m	mL/r	150
Total actuator volume	V_m	m^3	1.47×10^{-3}
Effective bulk modulus of system	β_e	Pa	7.0×10^8
Total leakage coefficient	C_{tm}	m^5/(N·s)	1.9×10^{-11}
Inertia of hydraulic motor and load	J_{m0}	kg·m^2	192.0625
Viscous damping coefficient	B_{m0}	N·s/m	800
External load torque	T_{L0}	N·m	214.9254

Table 2: Feedback values of stroke encoder.

Number	Input (m)	Initial cord length (m)	Final cord length (m)	Error (mm)
1	−0.01	0	−0.00942	−0.58
2	−0.1	−0.00942	−0.10951	0.09
3	−0.01	−0.10951	−0.11893	−0.58
4	0.1	−0.11893	−0.00942	9.51
5	−0.1	−0.00942	−0.10951	0.09
6	−0.01	0	−0.0106	0.6
7	−0.1	−0.0106	−0.11068	0.08
8	−0.01	−0.11068	−0.1201	−0.58
9	−0.1	−0.1201	−0.22019	0.09
10	−0.01	−0.22019	−0.22961	−0.58

Figure 7 shows the response of adaptive backstepping controller and Figure 8 shows the response of PID controller which has overshoot, and it is inadmissible in the leveling control of platform. It is indicated by the simulation results that compared with the conventional PID controller, the proposed controller performs better in controlling precision with external disturbance and uncertain parameters of the platform.

6.2. Individual Experiment. On the basis of digital simulation, we take an actual hydraulic winch to do the position servo control experiment with 15 tons external load using the adaptive backstepping controller. The equipments of individual experiment are shown in Figure 9.

The hydraulic winch realizes closed-loop control by stroke encoder. With respect to the requirement of high control precision, we set the input values as 0.01 m or 0.1 m under the inching mode of hydraulic winch. During the experiment, we select any point on the wire rope for stroke measurement and compare the result with input and the encoder feedback value. As a result of the "lowest point fixed angle error" leveling control scheme, the precision of wire rope draw-in is the focus of this experiment. The encoder feedback values are shown in Table 2, where the negative input signifies wire rope draw-in and the positive input signifies wire rope let-out.

The results of measurement on wire rope are shown in Figures 10 and 11, where Figure 10 shows the result of wire rope draw-in at 0.01 m, and Figure 11 shows the result of wire rope draw-in at 0.1 m.

The results of individual experiment indicate that under inching mode of the hydraulic winch, the error of wire rope draw-in is within 1 mm; however, the error of wire rope let-out obviously increases because of the overrunning load condition. Furthermore, the results prove that it is reasonable to ignore the variation of wire rope deformation. As a result of this, it can meet the high precision requirement of underwater platform leveling control with the "lowest point fixed angle error" leveling control scheme and adaptive backstepping controller.

6.3. Leveling Control Simulation. In this section, we carry out the leveling control simulation experiment of underwater platform using the hardware-in-loop simulation system connected with actual controller. We utilize the "lowest point fixed angle error" leveling scheme called "chase" to avoid the overrunning load condition of hydraulic winch for the platform leveling control based on the adaptive backstepping controller. The actual controller and hardware-in-loop system are shown in Figure 12.

We set the initial roll (ϕ) and pitch (θ) angles and survey the orientation of platform during the leveling control process. The results of hardware-in-loop simulation are shown in Figure 13, where Figure 13(a) shows $\phi > 0$ and $\theta > 0$, Figure 13(b) shows $\phi < 0$ and $\theta < 0$, Figure 13(c) shows $\phi < 0$ and $\theta > 0$, and Figure 13(d) shows $\phi > 0$ and $\theta < 0$.

The results of hardware-in-loop simulation indicate that the actual controller with adaptive backstepping arithmetic can effectively overcome uncertain parameters and external disturbance of hydraulic system to realize the leveling control of underwater platform based on "lowest point fixed angle error" leveling scheme. Besides, it proves the rationality of simulation model.

7. Conclusion

This paper presents a new underwater platform based on tension-leg platform. We have made simulation and experiment using the proposed adaptive backstepping controller. The results of digital simulation and individual experiment indicate that we can realize high precision position servo control of the actuator. Then, we utilize hardware-in-loop

simulation system to do leveling control simulation of the platform. It further proves robustness of the proposed controller with uncertain parameters and external load disturbance of system. Hence, this work paves the way for the actual leveling control of the platform.

Conflict of Interests

The authors declare that there is no conflict of interests regarding the publication of this paper.

Acknowledgments

This work was supported by the National Major Project (Grant no. 0261140024) and the National Natural Science Foundation (Grant no. 51079061).

References

[1] Y. J. Zhai and J. S. Ni, "The self-leveling method for six supports hydraulic platform on stationary base," *Journal of Southeast University*, vol. 26, no. 2, pp. 74–80, 1996.

[2] Y. Sheng and Y. Y. Qiu, "An automatic adjusting algorithm for the hydraulic platform with six legs," *Journal of Xidian University*, vol. 29, no. 5, pp. 593–597, 2002.

[3] Y. Sheng and Y. Y. Qiu, "Automatic leveling system of six supports hydraulic platform," *Hydraulics and Pneumatics*, no. 4, pp. 26–28, 1999.

[4] K. F. Ye, *Study on Leveling Control System With High Precision For platform Bearing Heavy Loads*, Chongqing University, 2004.

[5] F. Zhang, *Study on Leveling Control System of High Precision Platform*, Zhongbei University, 2008.

[6] S. E. Landsberger, *Design And Construction of A cable-Controlled parallel Link manipulator*, Massachusetts Institute of Technology, Cambridge, Mass, USA, 1984.

[7] S. Q. Fang, D. Franitza, M. Torlo, F. Bekes, and M. Hiller, "Motion control of a tendon-based parallel manipulator using optimal tension distribution," *IEEE/ASME Transactions on Mechatronics*, vol. 9, no. 3, pp. 561–568, 2004.

[8] M. Yamamoto, N. Yanai, and A. Mohri, "Trajectory control of incompletely restrained parallel-wire-suspended mechanism based on inverse dynamics," *IEEE Transactions on Robotics*, vol. 20, no. 5, pp. 840–850, 2004.

[9] C. B. Pham, S. H. Yeo, G. Yang, M. S. Kurbanhusen, and I.-M. Chen, "Force-closure workspace analysis of cable-driven parallel mechanisms," *Mechanism and Machine Theory*, vol. 41, no. 1, pp. 53–69, 2006.

[10] B. Zi, *Mechanics Analysis and Control Research of the Feed Tracking System For Super Antenna*, Xidian University, Xi'an, China, 2007.

[11] B. Wu, S. L. Wu, and K. D. Zhao, "Current status and development tendence of Stewart platform control strategy," *Machine Tool and Hydraulics*, vol. 10, pp. 5–7, 2005.

[12] C. Guan and S.-A. Zhu, "Multiple sliding mode robust adaptive control of an electro-hydraulic servo system," *Control Theory and Applications*, vol. 22, no. 6, pp. 931–938, 2005.

[13] C. Guan and S. Pan, "Adaptive sliding mode control of electro-hydraulic system with nonlinear unknown parameters," *Control Engineering Practice*, vol. 16, no. 11, pp. 1275–1284, 2008.

[14] A. Karimi and A. Feliachi, "Decentralized adaptive backstepping control of electric power systems," *Electric Power Systems Research*, vol. 78, no. 3, pp. 484–493, 2008.

[15] S.-Y. Ruan, G.-J. Li, X.-H. Jiao, Y.-Z. Sun, and T. T. Lie, "Adaptive control design for VSC-HVDC systems based on backstepping method," *Electric Power Systems Research*, vol. 77, no. 5-6, pp. 559–565, 2007.

[16] C. Hua, G. Feng, and X. Guan, "Robust controller design of a class of nonlinear time delay systems via backstepping method," *Automatica*, vol. 44, no. 2, pp. 567–573, 2008.

[17] T. I. Fossen, *Guidance and Control of Ocean Vehicles*, Wiley, New York, NY, USA, 1994.

[18] Q. Guo, Y. Liu, and Y. Liu, "Local structurization kinematic decoupling of six-leg virtual-axis NC machine tool," *IEEE/ASME Transactions on Mechatronics*, vol. 7, no. 4, pp. 515–518, 2002.

[19] B. Zi, B. Y. Duan, J. L. Du, and H. Bao, "Dynamic modeling and active control of a cable-suspended parallel robot," *Mechatronics*, vol. 18, no. 1, pp. 1–12, 2008.

[20] B. Zi, J. B. Cao, and Z. C. Zhu, "Design, dynamics, and workspace of a hybrid-driven-based cable parallel manipulator," *Mathematical Problems in Engineering*, vol. 2013, 15 pages, 2013.

[21] S.-R. Oh and S. K. Agrawal, "A reference governor-based controller for a cable robot under input constraints," *IEEE Transactions on Control Systems Technology*, vol. 13, no. 4, pp. 639–645, 2005.

[22] H. E. Merritt, *Hydraulic Control Systems*, Wiley, New York, NY, USA, 1976.

[23] J. L. Tang, *Research on Model-Based Adaptive Control of Six-Degree-of-Freedom Hydraulic Motion Platform*, Harbin Institute of Technology, Harbin, China, 2009.

[24] Y.-M. Fang, Y.-C. Han, L.-L. Zhao, and Q. Li, "Adaptive controller for electro-hydraulic servo system with uncertain coefficients in control input," *Control Theory and Applications*, vol. 26, no. 2, pp. 156–160, 2009.

[25] Y.-M. Fang, Z.-X. Jiao, W.-B. Wang, and P.-Z. Shao, "Adaptive backstepping sliding mode control for rolling mill hydraulic servo position system," *Electric Machines and Control*, vol. 15, no. 10, pp. 95–100, 2011.

[26] J. Ni and L. Peng, "An unified modeling on electro hydraulic poistion servo system and nonlinear control," in *Proceedings of the International Conference on Intelligent System Design and Engineering Application (ISDEA '10)*, pp. 268–272, October 2010.

[27] G. H. Xu, Z. L. Zeng, and F. Xie, "Dynamic modeling and control of a new underwater loading platform," in *Proceedings of the International Offshore and Polar Engineering*, vol. 2, pp. 406–410, Anchorage, Alaska, 2013.

[28] F. G. Ding, J. Wu, and Y. H. Wang, "Stabilization of an underactuated surface vessel based on adaptive sliding mode and backstepping control," *Mathematical Problems in Engineering*, vol. 2013, Article ID 324954, 5 pages, 2013.